engineering proceedings

MDPI

Proceeding Paper

Chlorophyll-A Time Series Study on a Saline Mediterranean Lagoon: The Mar Menor Case †

Arnau Garcá-i-Cucó [1,‡], José Gellida-Bayarri [1,‡], Beatriz Chafer-Dolz [2], Juan-Carlos Cano [1] and José M. Cecilia [1,*]

[1] Computer Engineering Department, Universitat Politècnica de València, Camino de Vera S/N, 46011 Valencia, Spain; agarcuc@inf.upv.es (A.G.-i.-C.); jgelbay@inf.upv.es (J.G.-B.); jucano@disca.upv.es (J.-C.C.)
[2] Biologic Crop Science, Calle Amadeo De Saboya 1 4, 46010 Valencia, Spain; bchafer@biologiccropscience.com
* Correspondence: jmcecilia@disca.upv.es
† Presented at the 10th International Conference on Time Series and Forecasting, Gran Canaria, Spain, 15–17 July 2024.
‡ These authors contributed equally to this work.

Abstract: The Mar Menor, Europe's largest saline lagoon, has experienced significant eutrophication. The concentration of chlorophyll-a (Chl-a) in the water is used as a critical indicator of this eutrophication process and can alert us to possible ecosystemic changes such as a massive fish die-off. The main objective of this paper is to predict chlorophyll-a concentration using various time series models. Among them, multivariate models such as short-term memory networks (LSTM) and, in particular, the autoregressive integrated moving average model with eXogenous variables (ARIMAX) demonstrated superior performance. These models incorporate multiple predictors, such as humidity, water temperature, conductivity and turbidity, thus capturing the complex interactions that affect Chl-a levels. Despite their effectiveness, these multivariate models introduce cascading errors due to the uncertainty inherent in the exogenous inputs. Consequently, the application of univariate models—such as Prophet, Triple Exponential Smoothing and ARIMA—are also studied for their relative robustness to error propagation.

Keywords: chlorophyll; coastal lagoon; eutrophication; fish kill; prophet; ARIMAX; LSTM

Citation: Garcá-i-Cucó, A.; Gellida-Bayarri, J.; Chafer-Dolz, B.; Cano, J.-C.; Cecilia, J.M. Chlorophyll-A Time Series Study on a Saline Mediterranean Lagoon: The Mar Menor Case. *Eng. Proc.* **2024**, *68*, 65. https://doi.org/10.3390/engproc2024068065

Academic Editors: Olga Valenzuela, Fernando Rojas, Luis Javier Herrera, Hector Pomares and Ignacio Rojas

Published: 25 September 2024

1. Introduction

The Mar Menor, Europe's largest saline lagoon, is located in Murcia, on the southwest coast of Spain. This lagoon, of great ecological, geological and scenic importance, is a vital habitat for several species and serves as a breeding and nursery ground for numerous shorebirds and marine organisms. It encompasses five volcanic islands—Barón, Perdiguera, Ciervo, Sujeto and Redonda—formed by marine currents that deposited sands and sediments, forming a narrow La Manga enclosing the ancient bay.

Beginning in 2015, the lagoon underwent a significant eutrophication process characterized by an increase in inorganic nutrients. This nutrient input, as documented in 2016, led to a substantial growth in phytoplankton populations, which clouded the waters and obstructed sunlight penetration, critically affecting the aquatic ecosystem. The resulting high phytoplankton density not only decreased underwater light, but also depleted oxygen levels, leading to the degradation of seagrass meadows. Seagrass meadows are essential for mediating nutrient exchange between the water column and sediments. Their degradation has significantly compromised the resilience of the ecosystem [1]. Further investigations between 2016 and 2018 indicated a partial recovery of benthic vegetation. However, in 2019, a major flood induced by an Isolated High Level Depression (ILD) event exacerbated the situation by increasing water turbidity and introducing large amounts of nitrates and phosphates. This incident triggered another severe algal bloom, colloquially known as the "Second Green Soup", and resulted in significant fish kill.

Despite efforts to restore its ecological balance, the Mar Menor continued to face challenges, with repeated fish kills recorded in subsequent years (2021 and 2022). Given that dissolved Chl-a is a proxy for phytoplankton concentration, this article aims to develop a predictive model for Chl-a levels that can reliably trigger alarms for excessive phytoplankton growth, thereby preventing ecological disasters. By integrating a range of environmental variables, including water temperature, humidity, conductivity and turbidity, our models have an enhanced predictive accuracy and offer a comprehensive view of the factors influencing eutrophication. Importantly, this research compares the efficacy of both multivariate and univariate models, providing valuable insights into their relative strengths and limitations in handling error propagation and model reliability. The findings from this study are expected to contribute to more effective monitoring and management strategies for the Mar Menor, ultimately aiding in the mitigation of ecological disruptions and promoting the sustainable health of this critical aquatic ecosystem.

The remainder of the paper is organized as follows: Section 2 provides an overview of the literature related to this study, outlining previous research efforts and contextualizing our contributions within the broader field. Following this, Section 3 employed in the research are detailed, establishing the empirical framework and analytical techniques utilized to achieve the study's objectives. Section 4 presents a comprehensive evaluation of the predictive models developed, including performance metrics and comparative analyses. The paper concludes with Section 5 that synthesizes the research findings, interprets their implications and proposes potential areas for future investigation.

2. Related Work

Recent shifts from oligotrophic to eutrophic states in several lagoons have stimulated a significant body of research on the dynamics of Chl-a concentrations, which are recognized as a key indicator of eutrophication processes [1–7]. Phytoplankton, the main cause of fish mortality and the "green soup" phenomenon, is closely related to Chl-a levels [1]. Furthermore, the relationship between phytoplankton concentration and water turbidity suggests that water clarity is an additional factor influencing Chl-A concentrations [1]. Nutrient levels, particularly phosphates and nitrates, also influence Chl-a levels because of their role in phytoplankton growth [2,3,8]. Existing studies confirm the seasonality of Chl-a time series while highlighting the modulation of Chl-a levels by various environmental factors, such as salinity and temperature [3,4]. Consequently, Chl-a concentrations exhibit distinct patterns in different ecosystems, such as those observed in the Bering Sea and the Lesser Sea [3,9]. In the Mediterranean climate of the Mar Menor, notable populations of diatoms (*Cylindroteca*) and dinoflagellates (*Prorocentrum*), together with recent changes in the populations of *Synechococcus Chlorophylae* and angiosperms, highlight the complex ecological dynamics influencing Chl-a levels [9].

Predictive modeling of Chl-a time series has increasingly employed deep learning techniques [10], with a focus on short-term memory (LSTM) networks. These models take advantage of prior data to refine predictions and have been applied in a variety of settings. Initial studies employing classical techniques such as ARIMA and basic neural networks found that models incorporating multivariate information often outperform simpler models [5]. For instance, research on the Small Prespa Lake utilized a combination of Convolutional Neural Network (CNN) and Long Short-Term Memory (LSTM) techniques, accounting for meteorological and water state variables over one or two preceding periods, achieving an R^2 of 87.4% [6]. Contrastingly, a study in the East China Sea, which included data from up to 15 days prior, used LSTM to predict Chl-a concentrations at four different geographic points, with an R^2 of 68.0% [7]. Both cases highlighted the challenges of dealing with asymmetric data distributions and pronounced seasonal peaks, which are also anticipated to be significant factors in our study. These insights into the variability and complexity of Chl-a prediction underscore the necessity for advanced modeling techniques capable of handling the non-linear and multifaceted nature of ecological data.

3. Materials and Methods

3.1. Framework

In the development of this project, it was imperative to obtain specific data sets relevant to the Mar Menor lagoon, focusing especially on chlorophyll concentration together with relevant climatological data. This integration is crucial for analyzing environmental interactions at both surface and subsurface levels, complemented by essential non-meteorological parameters such as date and time. The main source of data was a buoy located at 7 m depth in the deepest part of the lagoon, which has been operational since 14 October 2022. The buoy consists of a waterproof housing that encloses all electronic components and is anchored to a fixed location in the center of the lagoon [11]. It is equipped with solar panels and a battery to ensure a sustainable energy supply. Above the water surface, the buoy has an E+E Elektronik EE181 [12] sensor to measure air temperature and humidity, and an RM Young Wind Sentry anemometer [13] to assess wind speed. These sensors operate at a measurement frequency of approximately 30 s, aggregating data at 5 min, 60 min and 24 h intervals, with calculations for daily records that include extremes and variations in temperature and wind characteristics. The submerged components include six BETATHERM 100K6A372I thermistor temperature sensors (Betatherm Corporation, Shrewsbury, MA, USA) distributed at various depths (0.5 to 5 m) to record water temperature at the same frequency and averaging intervals as atmospheric sensors. In addition, three Aanderaa [14] oxygen sensors placed at 1, 3 and 6.5 m below the surface measure both temperature and dissolved oxygen content, designed to resist biofouling. Chl-a fluorescence and turbidity are monitored by a dual-channel SeaBird ECO [15] fluorometer (SeaBird, Bellevue, WA, USA), located 3 m below the water, which incorporates a mechanical scraper to prevent biofouling. All sensor data are collected, processed and recorded by a Campbell Scientific CR1000x data logger (Campbell Scientific, Logan, UT, USA) [16], which also handles data transmission via GPRS. System power management is monitored by a Campbell Scientific CH200 charge controller [17], which regulates the battery charge supplied by the solar panels and reports on power consumption, optimizing energy use across the buoy's systems.

3.2. Data Analytics Roadmap

As stated in Section 1, the main goal of this paper was to develop a model to predict the Chl-a time series evolution accurately. To do so, as with any time series, the researchers count on the Chl-a registries of the lagoon stored in hourly lapses. Nevertheless, this time series is not univariant, as many other variables have a massive impact on its values. Thus, it would be helpful for the modelling to consider more data, such as wind speed, water and air temperature, humidity, turbidity and conductivity. This information was obtained with the devices mentioned in the Section 3.1, stored with five minutes and hourly periodical registries. As depicted in the descriptive analysis in Figure 1, meteorological data, such as air temperatures, had a normal distribution, with maybe a mixed sample due to the seasons through the year, whereas seasonality was very noticeable and directly related to the sun exposure.

Other meteorological data also exhibited some patterns caused by several abnormal events, such as storms Denise and Efraín in December and November, which caused a massive decrease in humidity in the subsequent months, with January being the driest since 1961. Regarding wind speed, this paper only considered the average gust since the standard deviation and maximum gust had no meaningful relationship with the water's chlorophyll-a concentration. For the same reason, derivated variables such as vapour pressure were excluded from the research. This average wind had a positive asymmetry, with the feature achieving some high values and mostly being low. These peaks almost always happened in the same hourly periods, marking the seasonality. In addition, the data were more unstable in November and December, which are the more climatologically unstable months in the year in the area.

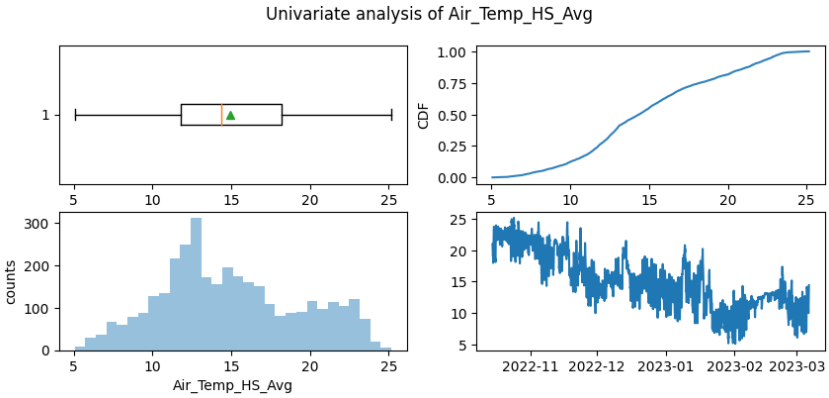

Figure 1. Air temperature analysis.

As for the water variables, the temperature was mostly stable at all different depths, even though some sensors were frequently aberrant. In Figure 2, note how the trend marks a two-year seasonality and how the sunlight causes a mild seasonality. With respect to oxygen saturation (a more understandable metric than oxygen concentration), the registries showed that the Efraín and Denise storms also caused a fall in November and December. The same climatological events also caused a decrease in corrected conductivity in November and December (a stable variable not dependent on other variables such as water temperature) and an increase in turbidity in mid-January and late February. This last variable, turbidity, also exhibited several daily seasonal patterns, probably caused also by the sunlight effect. Lastly, it is necessary to note that another minimum in oxygen saturation was registered in March 2023 without any meaningful storm nearby in the historical registries.

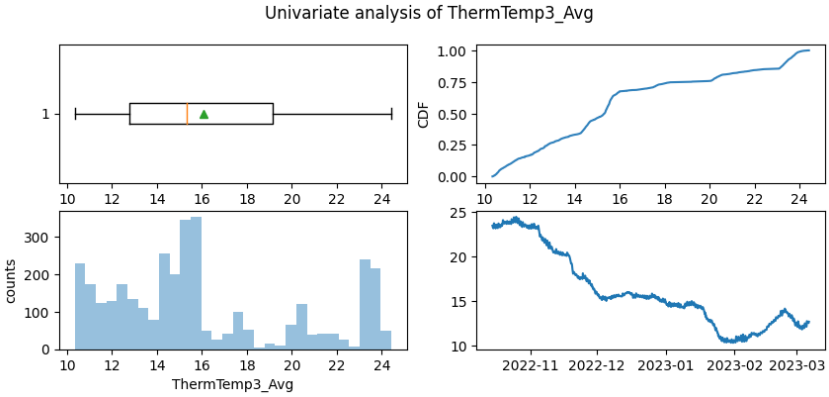

Figure 2. Water temperature analysis.

The chlorophyll-a also had a mainly daily seasonal pattern, as depicted in Figure 3, and the Denise and Efraín rainfalls were again observable in the data in the shape of peaks in November and December, respectively.

Finally, as previously said, the system was multivariate, with several variables being interconnected. As such, a profound study on the meaningful relationship between time series was due (see Figure 4). The more evident relationships were the ones involving the water and air temperatures. Furthermore, temperature also impacted the water's conductivity, even though the metric had been corrected. The water temperature was also related to the oxygen saturation, at least on the lagoon's surface and, for some reason, the wind speed and oxygen saturation at 3 m under the surface also shared a link, even though this one may be spurious.

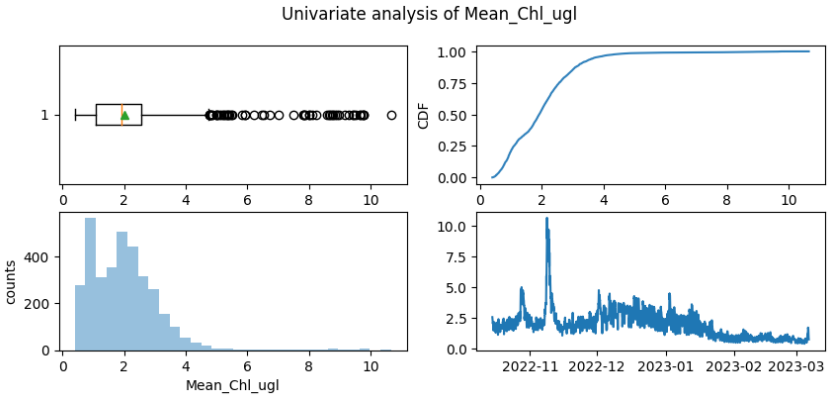

Figure 3. Chlorophyll-a analysis.

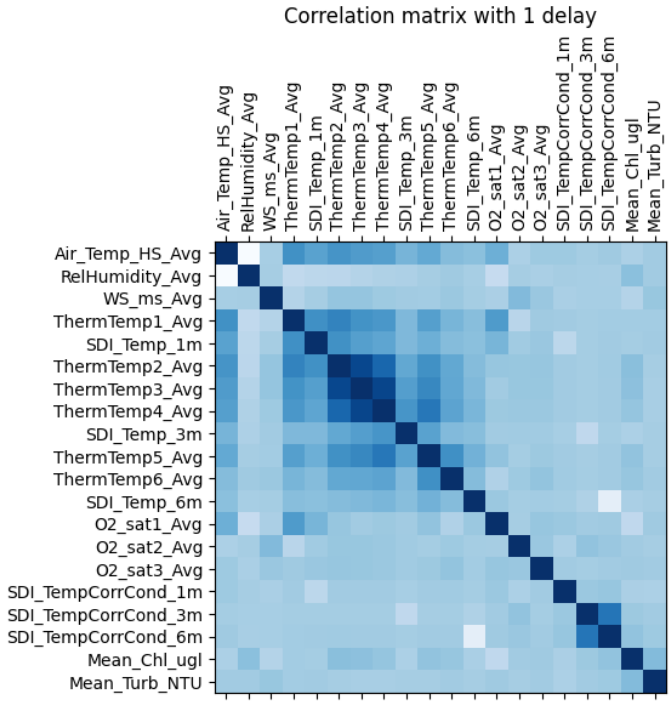

Figure 4. Feature correlation matrix. Stronger blue color shows a higher correlation between variables.

Despite this, the most crucial variable to study, Chl-a, had a mild relationship with all the other variables. Despite that, the links with humidity, water temperature, turbidity and conductivity were vital.

After preprocessing the data and breaking down all the interdependences between variables, deciding which approach to use for developing the models was imperative. In this case, an ensemble composed of several other models was proposed. One was an exponential smoothing-based model [18]. In this concrete problem, this univariate technique must consider the time series seasonality to perform at its best. As such, it was suggested to use the *triple exponential smoothing-based model*, determined by the following formula:

$$F_{t+m} = (S_m + m \cdot b_t) \cdot E_{t+m-s}$$

In this case, F represents the smoothing of the series, S represents the mobile average or level, b represents the tendency, and E represents the seasonality at the moment where it is inferred.

The second univariate model proposed was Meta's *Prophet* [19]. This estimator, mainly used for businesses, uses trend (g), seasonality (s) and holidays (h) according to the following formula:

$$y(t) = g(t) + s(t) + h(t) + \epsilon_t$$

Finally, the last approach taken was the auto-regressive integrated moving averages model (*ARIMA*) [18]. This widespread model, which follows the Box and Jenkins methodology, consists of two models. One linear regressor uses the previous autocorrelated data to develop a prediction, whereas the moving averages smooth the errors. To overcome the non-stationarity problem, a lag is frequently used, resulting in the integrated model. The proper formula would be:

$$\nabla^d Y_t = ARMA(p,q) = c + \sum_{i=1}^{p}(\phi_i \nabla^d Y_{t-i}) + a_t - \sum_{i=1}^{q}(\theta a_{t-i})$$

or simply

$$\phi_p(B)\nabla^d Y_t = c + \theta_q(B)a_t$$

In this equation, ϕ and θ are hyperparameters that need to be optimized, and p, d, q is the ARIMA model order. At the same time, Y_t and a_t are the time series and the random component values in the period t, respectively.

To also include exogenous variables (X), that is, other time series, the ARIMA can be enhanced into an *ARIMAX* [18] model, becoming:

$$Y_t = c + \beta X_t + e_t$$

where e_t behaves as an ARIMA(p, d, q).

Finally, a neural network-based approach was taken. Specifically, an *LSTM* [20] was used to address the intrinsic patterns in data using feedback from hidden layers obtained in previous iterations, hence non-linear relationships with the previous results disclosed in the final prediction were disclosed.

4. Discussion and Evaluation

The primary objective of the experimental process was to optimize the models and then compare them to determine the most effective ensemble. The approach involved developing a rolling Mean Absolute Percentage Error (MAPE) technique to identify which model would perform best for specific predictions. The ensemble comprised models with the fewest errors for each prediction. Initially, different models were optimized based on their Root Mean Square Error (RMSE) performance index, which penalizes larger errors more significantly than smaller ones.

An extensive study was conducted involving Holt–Winters models with both additive and multiplicative seasonalities and trends. The optimal model was the Holt–Winters with a multiplicative trend and additive seasonality, achieving an RMSE of 0.1967 µg/L.

For the Prophet model, experiments considered the nature of seasonality and trend (linear, multiplicative or non-existent) and whether the model should be lagged. The best-performing Prophet model was non-lagged, with a linear trend and multiplicative seasonality, achieving an RMSE of 0.7595 µg/L.

Two ARIMA models were examined: ARIMA(0, 1, 1) (0, 1, 2)24 and ARIMA(1, 1, 5). Both followed the residual assumptions, and their errors were confirmed to be white noise. The ARIMA(0, 1, 1) (0, 1, 2)24 model yielded better results with an RMSE of 0.2048 µg/L.

For the multivariate models, exogenous variables most correlated with Chl-a, such as humidity, water temperature, water conductivity at 6 m depth and turbidity, were used. Among the multiple temperature-related variables, only the temperature at a depth of 1.5 m was considered, as it showed the highest correlation with Chl-a.

The ARIMAX model adopted the ARIMA(0, 1, 1) (0, 1, 2)24 structure, with experimentation focused on the combination of variables used. The optimal model included all the correlated variables mentioned earlier, achieving an RMSE of 0.1951 µg/L.

For the LSTM model, various architectures and numbers of previous records (1 day, 3 days and 1 week) were tested to develop the best-performing model. The optimal configuration used the previous 3 days' entries and three layers of 40, 30, and 24 cells with 20% dropout, achieving an RMSE of 0.6056 µg/L.

Finally, the models were assessed using a rolling window, and the MAPE metric was employed to identify the most promising predictions for each period. To forecast the next 24 h of Chl-a evolution, the window size was determined (see Figure 5).

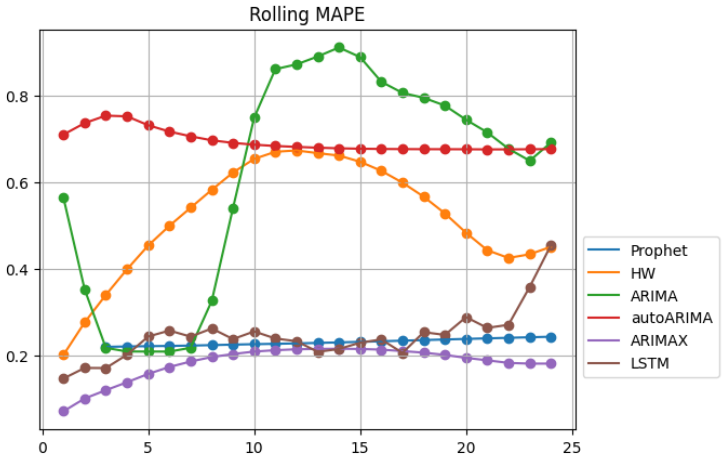

Figure 5. Rolling MAPE.

The MAPE results indicated that the LSTM model provided the best predictions for 13 and 17 h ahead, while the ARIMAX model performed better in all other cases. None of the models exceeded an MAPE of 25%. However, as exogenous variables are random and not controllable, multivariate techniques might cause error accumulation when forecasting, unlike univariate models.

Examining the univariate models' results in Figure 6, it is evident that the Holt-Winters model performs best for the first two hours, despite the second hour showing the worst performance in the ensemble with approximately 30% MAPE. The ARIMA model dominates the next four hours (third to seventh predictions), maintaining the MAPE below 25%. From the eighth to the twenty-fourth predictions, the Prophet model performed best, with the MAPE gradually increasing to 25% by the twenty-fourth hour.

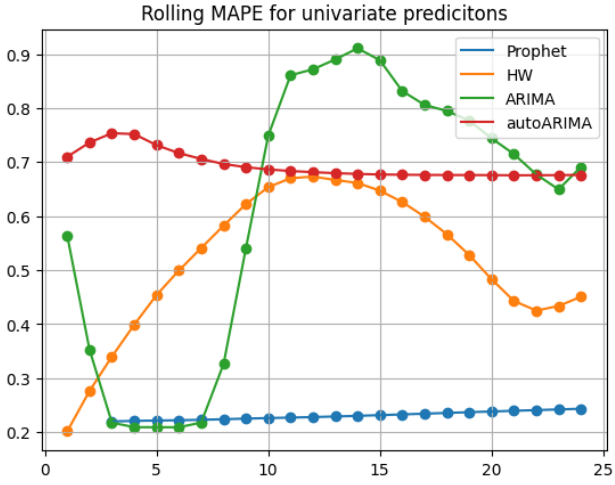

Figure 6. Rolling MAPE for univariate predictions.

5. Conclusions

In this study, we developed predictive models that, in the most favorable scenarios, achieve an RMSE of approximately 0.2. These predictions were primarily derived using ARIMAX models, and in certain instances, through LSTM neural networks. A significant limitation of these multivariate approaches is their reliance on exogenous variables, which are themselves subject to variability. This dependency introduces a propagation of errors, as the prediction accuracy of exogenous variables directly influences the overall model accuracy. Consequently, this study highlights the utility of univariate models, notably the Prophet model, which demonstrated comparable precision to its multivariate counterparts.

Furthermore, this research identifies opportunities for enhancing the spatial resolution of environmental data within the Mar Menor lagoon by integrating additional oceanographic buoys. Such enhancements would more accurately reflect the lagoon's heterogeneous ecological dynamics. It is also recommended to increase the dataset with additional biogeochemical and physical parameters, including but not limited to water currents, sea levels and chemical concentrations of nitrates and phosphates. These additions are anticipated to further refine the predictive capability of the models. Lastly, it is noteworthy that the available dataset does not encompass a complete annual session, thereby limiting our ability to fully determine the seasonal patterns typically associated with weather changes. Nevertheless, certain variables within the dataset exhibited trends that likely correspond to annual seasonality, suggesting an underlying periodic influence on the observed time series.

Author Contributions: Conceptualization, A.G.-i.-C. and J.G.-B.; methodology, A.G.-i.-C.; software, A.G.-i.-C. and J.G.-B.; validation, A.G.-i.-C., J.G.-B. and B.C.-D.; formal analysis, A.G.-i.-C.; investigation, A.G.-i.-C.; resources, J.M.C.; data curation, A.G.-i.-C.; writing—original draft preparation, A.G.-i.-C. and J.G.-B.; writing—review and editing, B.C.-D., J.M.C. and J.-C.C.; visualization, A.G.-i.-C.; supervision, B.C.-D., J.M.C. and J.-C.C.; project administration, J.M.C. and J.-C.C.; funding acquisition, J.M.C. and J.-C.C. All authors have read and agreed to the published version of the manuscript.

Funding: This work has been funded by the projects TED2021-130890B, funded by MCIN/AEI/10.13039/501100011033 and by the European Union NextGenerationEU/PRTR, Ramon y Cajal Grant RYC2018-025580-I, "FSE invest in your future" and "ERDF A way of making Europe" and the European Union's Horizon 2020 research and innovation programme under grant agreement No. 101017861.

Institutional Review Board Statement: Not applicable.

Informed Consent Statement: Not applicable.

Data Availability Statement: The data presented in this study are available upon request from the corresponding author.

Conflicts of Interest: The authors declare no conflicts of interest.

References

1. Sandonnini, J.; Del-Pilar-Ruso, Y.; Cortés-Melendreras, E.; Giménez-Casalduero, F. Massive aggregations of serpulidae associated with eutrophication of the mar menor, southeast iberian peninsula. *Front. Mar. Sci.* **2020**, *7*, 531726. [CrossRef]
2. Li, P.; Zhao, N.; Zhou, D.; Cao, M.; Li, J.; Shi, X. Multivariable time series prediction for the icing process on overhead power transmission line. *Sci. World J.* **2014**, *2014*, 256815. [CrossRef] [PubMed]
3. Mozetič, P.; Solidoro, C.; Cossarini, J.; Socal, G.; Precali, R.; Francé, J.; Bianchi, F.; De Vittor, C.; Smodlaka, N.; Fonda Umani, S. Recent trends towards oligotrophication of the northern adriatic: Evidence from chlorophyll a time series. *Estuaries Coasts* **2010**, *33*, 362–375. [CrossRef]
4. Niebauer, J.H.; Alexander, V.; Henrichs, M.S. A time-series study of the spring bloom at the bering sea ice edge i. physical processes, chlorophyll and nutrient chemistry. *Cont. Shelf Res.* **1995**, *15*, 1859–1877. [CrossRef]
5. Schalles, F.J.; Gitelson, A.A.; Yacobi, Z.Y.; Kroenke, E.A. Estimation of chlorophyll a from time series measurements of high spectral resolution reflectance in an eutrophic lake. *J. Phycol.* **2002**, *34*, 383–390. [CrossRef]
6. Cen, H.; Jiang, J.; Han, G.; Lin, X.; Liu, Y.; Jia, X.; Ji, Q.; Li, B. Applying deep learning in the prediction of chlorophyll-a in the east china sea. *Remote Sens.* **2002**, *14*, 5461. [CrossRef]

7. Barzegar, R.; Aalami, M.T.; Adamowski, J. Short-term water quality variable prediction using a hybrid cnn–lstm deep learning model. *Stoch. Environ. Res. Risk Assess.* **2020**, *34*, 415–433. [CrossRef]
8. Ouaissa, S.; García-Gómez, C.; Moreno-Ostos, E.; Mercado-Carmona, J.M. Variabilidad del fitopláNcton en la Laguna Costera mar Menor Durante un Periodo de Eutrofización Severo. Available online: https://agris.fao.org/search/en/providers/122367/records/6474804cbf943c8c79883d30 (accessed on 26 August 2024).
9. Mercado, J.M.; Cortés, D.; Gómez-Jakobsen, F.; García-Gómez, C.; Ouaissa, S.; Yebra, L.; Ferrera, I.; Valcárcel-Pérez, N.; López, M.; García-Muñoz, R.; et al. Role of small-sized phytoplankton in triggering an ecosystem disruptive algal bloom in a mediterranean hypersaline coastal lagoon. *Mar. Pollut. Bull.* **2021**, *164*, 111989. [CrossRef] [PubMed]
10. Xu, J.; Hu, Y.; Liu, H.; Mi, W.; Li, G.; Guo, J.; Feng, Y. A novel multivariable time series prediction model for acute kidney injury in general hospitalization. *Int. J. Med. Informatics* **2022**, *161*, 1386–5056. [CrossRef] [PubMed]
11. Pierson, D. Innovative Modelling Approaches for Predicting Socio-Environmental Evolution in Highly Anthropized Coastal Lagoons. Available online: http://www.smartlagoon.eu/wp-content/uploads/2021/11/SMLG_D2.1_Report-on-sensing-technologies_VF.pdf (accessed on 26 August 2024).
12. E+E Elektronik EE181 Air Temperature and Humidity Sensor. Available online: https://www.campbellsci.com/ee181-l (accessed on 26 August 2024).
13. RM Young Wind Sentry Anemometer. Available online: https://www.campbellsci.com/03101-sentry-anemometer (accessed on 26 August 2024).
14. SeaBird ECO Dual Channel Fluorometer. Available online: https://www.seabird.com/eco-flntu/product?id=60762467722 (accessed on 26 August 2024).
15. Aanderaa Oxygen Sensors. Available online: https://www.aanderaa.com/oxygen-sensors (accessed on 26 August 2024).
16. CR1000X: Measurement and Control Datalogger. Available online: https://www.campbellsci.com/cr1000x (accessed on 26 August 2024).
17. CH200: Smart 12 V Charging Regulator. Available online: https://www.campbellsci.com/ch200 (accessed on 26 August 2024).
18. Díaz, J.C.G. *Series Temporales, Análisis, Predicción, Ejercicios Prácticos*; Universidad Politécnica de Valencia: Valencia, Spain, 2011.
19. Taylor, S.J.; Letham, B. Forecasting at scale. *PeerJ* **2017**, *5*, e3190v2. [CrossRef]
20. Hochreiter, S.; Schmidhuber, J. Long short-term memory. *Neural Comput.* **1997**, *9*, 1735–1780. [CrossRef] [PubMed]